

Reduction of the RF Loss in the Garnet Material of a Tunable Cavity by Optimizing the Magnetic Field Distribution Using Shimming

I. Terechkine and G. Romanov

It was mentioned in earlier notes [1÷4] that the high RF power loss in the tuner is closely associated with the low level of the static magnetic field in the garnet and resulting sharp increase of magnetic permeability in the garnet (both the real and the imaginary parts) in the vicinity of the gyromagnetic resonance. One of ways to improve the quality of the field is by using magnetic shimming. Shimming the poles of the flux return of the bias magnet do not provide desirable effect because the gap between the pole and the garnet material of the cavity tuner in the proposed design is relatively large (see geometry of the cavity in Fig. 1 of [4]). Another option, which will be investigated in this note, is using shims installed in the close vicinity of the tuner. In this case, the material of the shims must be low loss, so using garnet looks like a natural choice. Generally, the type of the garnet can be different from what is used in the tuner; in this case, we have chosen to use the same AL-800 type. First attempts of adding the shims did show significant improvement in the uniformity of the magnetic field and permeability in the garnet. Some modest optimization efforts resulted in the shape of the shim shown in Fig. 1-b; this ring-shaped shim is 3.5 mm thick with 115 mm inner radius and 148 mm outer radius. The edges of the shim that are not in the direct contact with the tuner are rounded: fillet radius $r = 2.5$ mm. Fig. 1-a shows the magnetic field map at the top of the tuner in the initial configuration (no shims) at 6.0 kA bias current; it must be compared with similar map with added shim in Fig. 1-b. The minimum value of the magnetic field has increased from ~33 Oe to ~50 Oe; no direct gyromagnetic resonance condition exists in the garnet material any more. Fig. 1-c shows 3D view of the tuner with the ring-type shim.

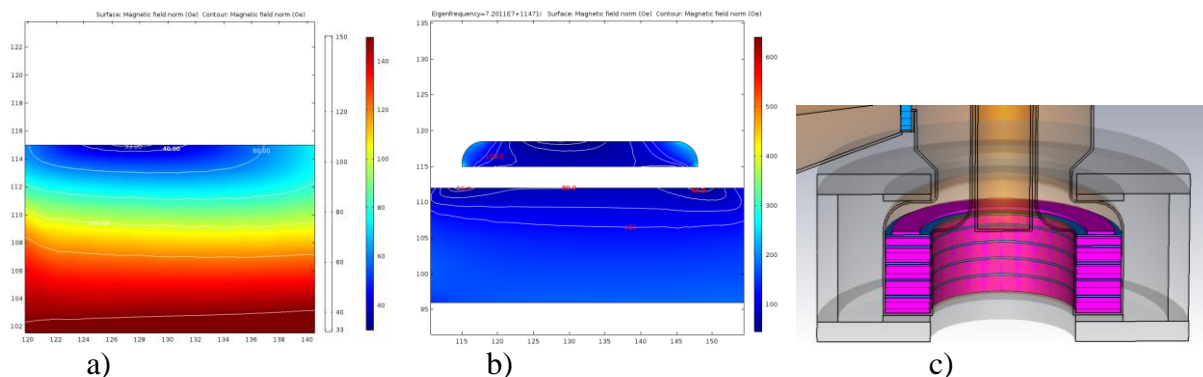


Fig. 1. Initial (a) and optimized (b) configuration of the top of the tuner, c) 3D view of the optimized tuner model.

In Fig. 2 permeability and static RF power loss density are shown in the top part of the tuner with the shim for the same 6 KA bias. Areas with relatively high power loss densities became smaller in volume; the value of the power loss is also smaller.

Lower power loss density in the first (top) block of the tuner makes it possible increasing thickness of this block (it was 13.5 mm in [3] and [4]). We will use the following configuration of the tuner: the first block is 16 mm thick, all the rest are 21 mm thick each. The total length of the tuner is 100 mm now.

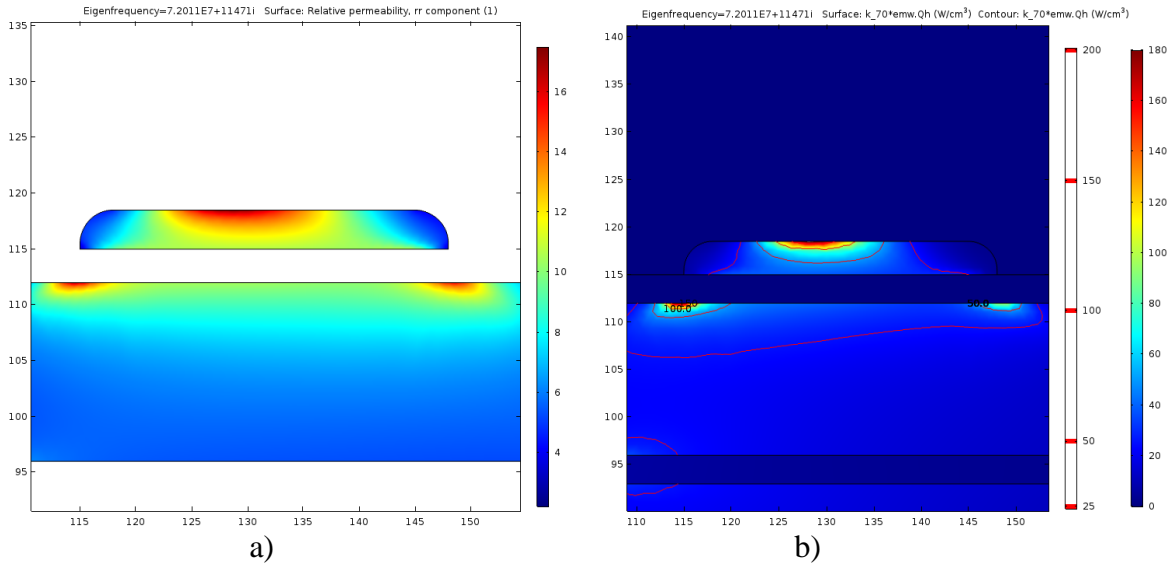


Fig. 2. Permeability a) and static RF power loss density b) at the 6 kA bias current

Following the analysis pattern used in [3] and [4], before evaluating the temperature field in the tuner with this new configuration, static analysis of the RF losses was performed. As the second harmonic cavity will be used only during two three-millisecond intervals, let's identify the frequencies corresponding to these intervals. Tables 1 and 2 provide this information.

Table 1. Frequency change during the 1-st three-millisecond interval of the ramp

t (ms)	0	0.5	1.0	1.5	2.0	2.5	3.0	3.5
f (MHz)	75.73	75.90	76.41	77.24	78.34	79.68	81.20	82.85

Table 2. Frequency change during the 2-nd three-millisecond interval (104.5 MHz transition frequency is in the middle of the interval)

t (ms)	15.5	16.0	16.5	17.0	17.5	18.0	18.5	19.0	19.5
f (MHz)	103.99	104.16	104.31	104.44	104.57	104.67	104.77	104.86	104.94

Table 3 summarizes results of the static RF power loss modeling corresponding to the first interval. Current setting resulting in the needed frequency at each discrete time moment, power conversion coefficient, and the heating power generated in the top block (B1), top disc (D1), and in the shim are shown.

Table 3. Static RF power loss during the 1-st 3-ms interval

t (ms)	0	0.5	1.0	1.5	2.0	2.5	3.0	3.5
I _w (kA)	6.6625	6.69	6.765	6.90	7.08	7.32	7.60	7.94
f (MHz)	75.73	75.914	76.402	77.256	78.341	79.7	81.175	82.827
U _{gap}	56.495	56.527	56.613	56.764	56.960	57.21	57.488	57.809
K _P · 10 ⁻⁶	3.133	3.1296	3.1201	3.1035	3.0822	3.0553	3.0258	2.9923
B1 (W)	7103	7041	6885	6628	6325	5970	5608	5230
D1 (W)	461	461	460.5	459	457	454	450	445
Shim (W)	890	870	818	742	663	587	525	470

In Table 4, similar information for the second interval can be found. The power density distribution during the second interval stays substantially unchanged, so fewer intermediate points are needed to get desired accuracy of the average power calculation.

Table 4. Static RF power loss during the 2-nd 3-ms interval

t (ms)	16.0	17.0	17.5	19.0
I _w (kA)	16.7	17.0	17.1	17.4
f (MHz)	104.05	104.42	104.53	104.88
U _{gap}	62.714	62.809	62.84	62.932
K _P · 10 ⁻⁶	2.5426	2.5349	2.5324	2.525
B1 (W)	2564	2534	2524	2495
D1 (W)	334	331.5	331	328
Shim (W)	196	193.2	192.5	190

Figure 3 shows how the static power loss in the top block of the tuner changes with time during the 1-st and the 2-nd intervals. For the 1-st interval, the static power loss in the shim is also shown (scaled 10 times up, blue curve).

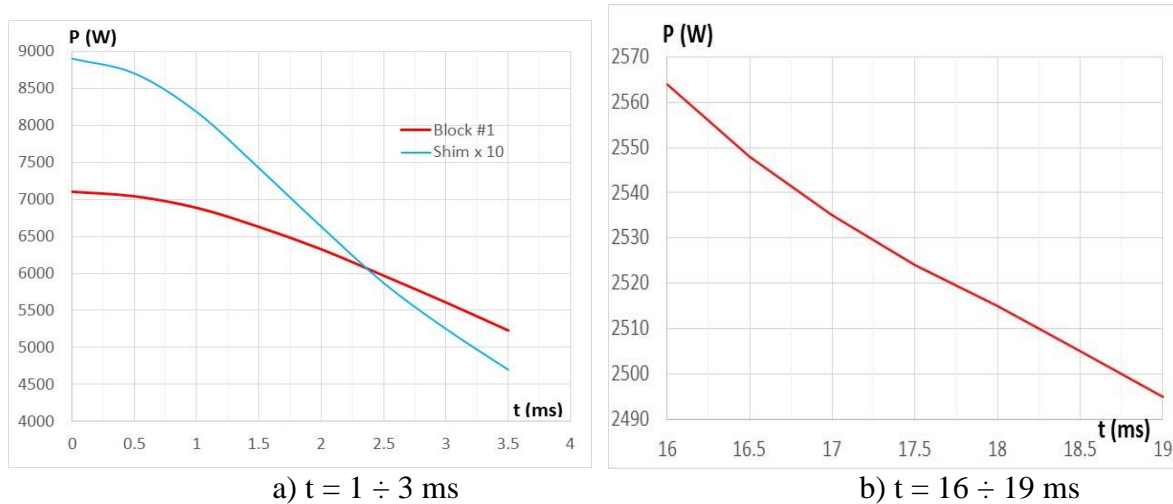


Fig. 3. Power dissipation in the 1-st block during the two active intervals

Data in tables 3 and 4 can be used to calculate the average power dissipated in the top block (#1), in the top disk, and in the shim. The time-averaged heat deposition in the block #1 during the 1÷3 ms interval is ~300 W. During the 16÷19 ms interval it is ~115 W, so the total average power in the block #1 is ~415 W. For the previously studied case with no shimming the heating power for the top block was 436 W [4]; one should also take into consideration that in that case the block was 13.5 mm thick.

The average heat deposition in the shim during the 1÷3 ms interval is ~31.5 W. During the 16÷19 ms interval it is ~9 W, so the total average power in the shim is ~40 W. The average heat deposition in the top alumina disk during the 1÷3 ms interval is ~21 W. During the 16÷19 ms interval it is ~15 W, so the total average power in the disk #1 is ~36 W.

To evaluate temperature in the top portion of the tuner, we need to use the average power density distribution in the parts of the tuner. Let's investigate what the power loss distribution is for the bias current I_w = 6.6625 kA, which corresponds to the frequency f = 75.73 MHz.

Graphs in the Fig. 4a show the RF loss power density in W/cm^3 along the radial lines near the top, near the bottom, and at the center of the top block. RF loss power density distribution along the top of the shim is also shown here for reference (red curve). Fig. 4b shows the power loss graphs along the vertical lines aligned with the peaks in Fig. 4a: $R = 113$ mm and $R = 150$ mm.

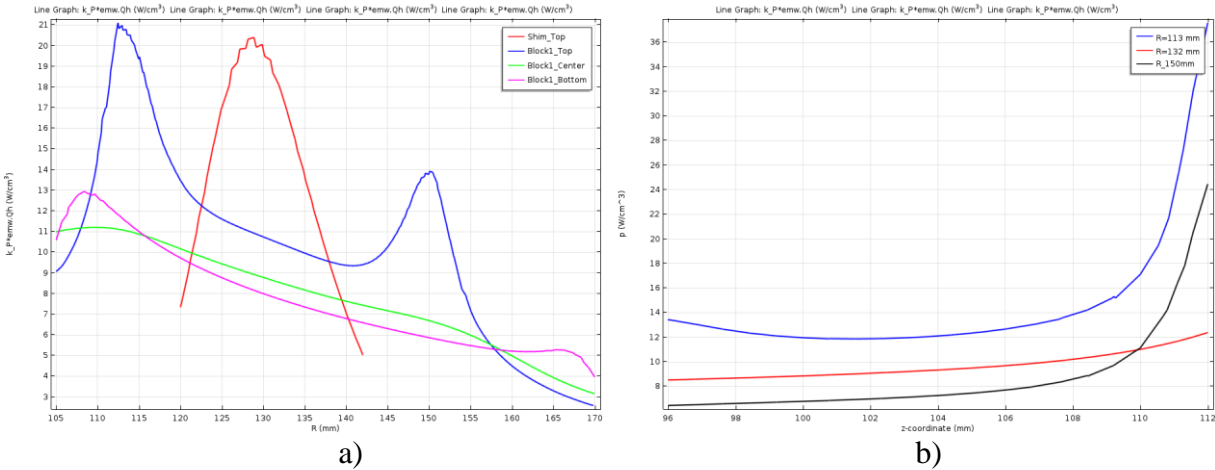


Fig. 4. RF loss power density plots along the radial (a) and vertical (b) lines in the cross-section of the top block (W/cm^3).

The sizes of the volumes with the peaks of power in the graphs typically are 15 mm radially and 2 mm vertically. Off these anomalous volumes, the power density distribution can be described (with some reserve) by the following expression

$$p(r) = 30 - 0.153 \cdot r,$$

where the radius r is in **mm** and the power density p is in W/cm^3 . Some changes along Z are neglected here. For the anomalous areas, we will extract the average power density directly from the model.

Distribution of the heating power in the shim is shown in Fig. 5. Calculated average power density in the shim is $8.6 W/cm^3$. In the top central portion it is $16.7 W/cm^3$.

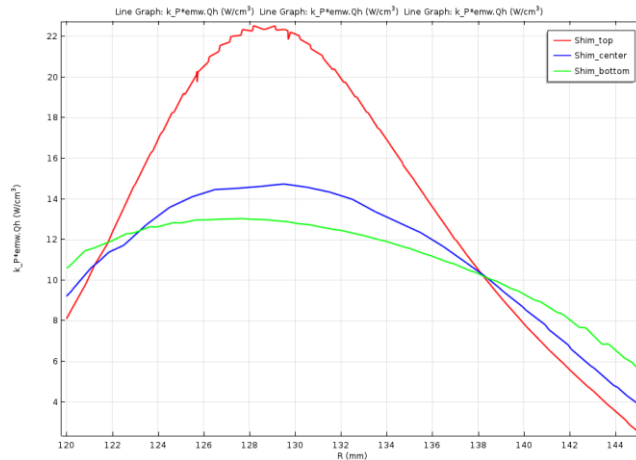


Fig. 5. RF loss power density plots along the radial lines in the cross-section of the shim (W/cm^3).

RF loss power density in the second garnet block is shown in Fig. 6

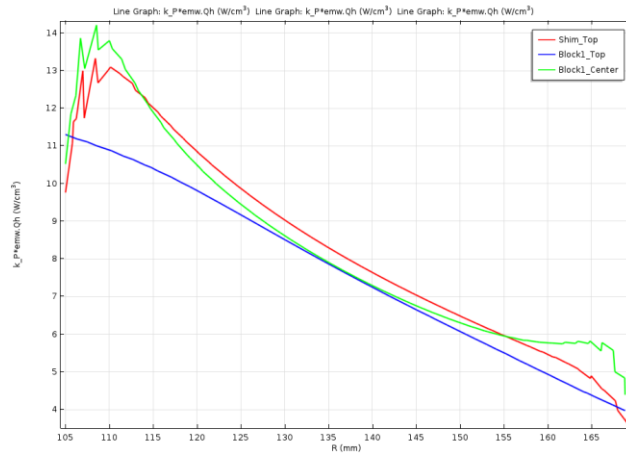


Fig. 6. RF loss power density plots along the radial lines in the cross-section of the second block (W/cm^3).

The heating power density in the second block can be expressed as a function of the radius by the expression

$$p(r) = 25.4 - 0.123 \cdot r \tag{1/}$$

Some variations along Z axis are neglected here; r is in **mm**, and p is in W/cm^3 .

Heating power density in the disks #1, #2, and #3 (except the anomalous loss area in disk #1) can be approximated by the following expressions (**mm and W/cm^3**):

Disk 1: $p(r) = 8 - 0.0385 \cdot r$ (for $r > 117.5$ mm) /2/

Disk 2: $p(r) = 6.5 - 0.031 \cdot r$ /3/

Disk 3: $p(r) = 4.4 - 0.02 \cdot r$ /4/

Graphs comparing the power density distribution in the alumina disks #1 and #2 are shown in Fig. 7a. Fig. 7b shows a map of the RF losses in the blocks, disks, and in the shim.

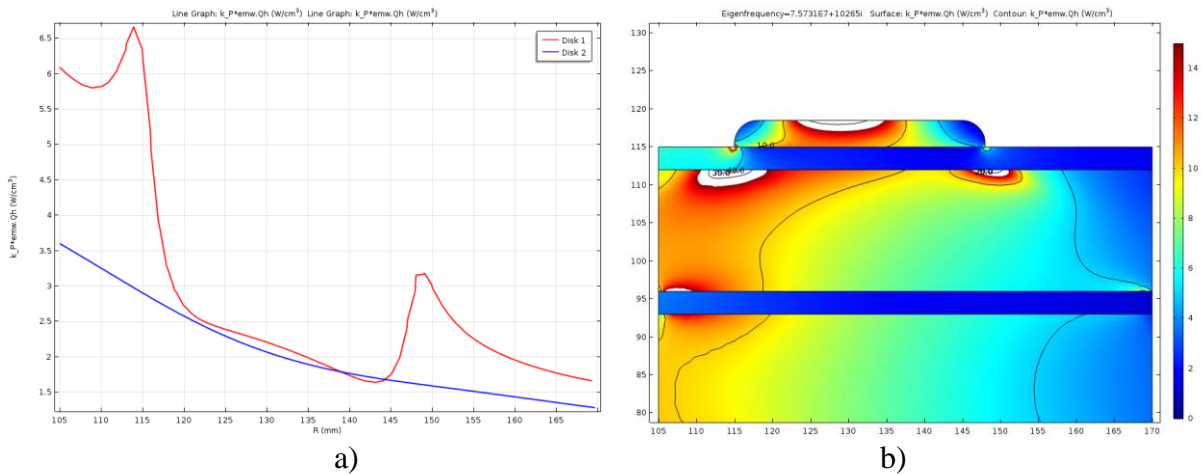


Fig. 7. a) RF loss power density in the alumina disks #1 and #2 (W/cm^3). b) Map of the RF losses in the blocks, disks, and in the shim.

There are two anomalous areas in the first alumina disk. We will neglect one at R = 150 mm as it is relatively small. The area ending at R ≈ 117.5 mm will be treated as a separate zone with an average power density. We also see that two anomalous areas in the block #1 also require individual treatment in the form of specially cut areas; the average power densities in these areas will be found by direct modeling.

As a result of the power loss distribution analysis during the first millisecond of the bias current ramp made above, we were able to come to the analytical expressions of the RF loss power density as functions of the radius for some parts of tuner (expressions /1/ to /4/). Also for this 1-ms interval starting at t = 0 we have four additional zones where it was difficult to find an analytical expression, so the average power density in these areas was found by direct modeling instead:

Central top area of the shim	16.7 W/cm ³
Inner portion of the disk #1	6.55 W/cm ³
Inner peak loss area in block #1	17.92 W/cm ³
Outer peak loss area in block #1	11.73 W/cm ³

The data obtained this way was applied for the first 1-ms interval to find the average density of the energy deposition. Similar approach was used to find distribution of the static RF heating power corresponding to the second (starting at 1 ms, I_w = 6.765 kA, f = 76.41 MHz) and third (starting at 2 ms, I_w = 7.08 kA, f = 78.34 MHz) 1-ms intervals.

Table 5 summarizes results of calculation of the energy density deposited in the elements of the model during the three 1-ms time intervals, in **J/cm³**. Inside each time interval, the highest value of the losses in the beginning of the interval (0 ms, 1 ms, and 2 ms) was assumed. The last column in the table shows the sum of the three preceding columns, that is the heat deposited in the elements of the tuner during the first 3-ms interval.

Table 5. Energy density in the elements of the tuner during the first 3-ms interval

Element	0 – 1 ms	1 - 2 ms	2 – 3 ms	0 – 3 ms
Disk1	10 ⁻³ *(8-0.038*r)	10 ⁻³ *(8-0.0385*r)	10 ⁻³ *(7.3 – 0.0346*r)	10 ⁻³ *(23.3-0.111*r)
Disk1_add	6.55e-3	6.57e-3	6.60e-3	19.72e-3
Disk 2	10 ⁻³ *(6.5-0.031*r)	10 ⁻³ *(5.9-0.023*r)	10 ⁻³ *(7.3 – 0.0346*r)	10 ⁻³ *(19.7-0.089*r)
Disk 3	10 ⁻³ *(4.4-0.02*r)	10 ⁻³ *(3.6-0.0154*r)	10 ⁻³ *(4.3 – 0.0192*r)	10 ⁻³ *(12.3-0.055*r)
Shim	8.6e-3	8.06e-3	6.9e-3	23.6e-3
Shim_add	16.7e-3	15e-3	11.5e-3	43.2e-3
Block1	10 ⁻³ *(30–0.153*r)	10 ⁻³ *(30–0.153*r)	10 ⁻³ *(30–0.153*r)	10 ⁻³ *(90–0.46*r)
Block1_1add	17.92e-3	17.92e-3	15.1e-3	51e-3
Block1_2add	11.73e-3	11.73e-3	9.4e-3	33e-3
Block2	10 ⁻³ *(25.4 – 0.123*r)	10 ⁻³ *(25.4 – 0.123*r)	10 ⁻³ *(25.4 – 0.123*r)	10 ⁻³ *(76.2 – 0.37*r)

Similar approach can be used to find the average power for the second time interval from 16 to 19 ms. Heat deposition distribution practically is not changing during this 3-ms interval, so the data corresponding to t = 17.5 ms (I = 17 kA, f = 104.57 MHz) will be used for the averaging. Figures 8 and 9 show RF loss power density spatial distribution in the shim, the disks (#1, #2, and #3), and the blocks (#1 and #2) at this moment.

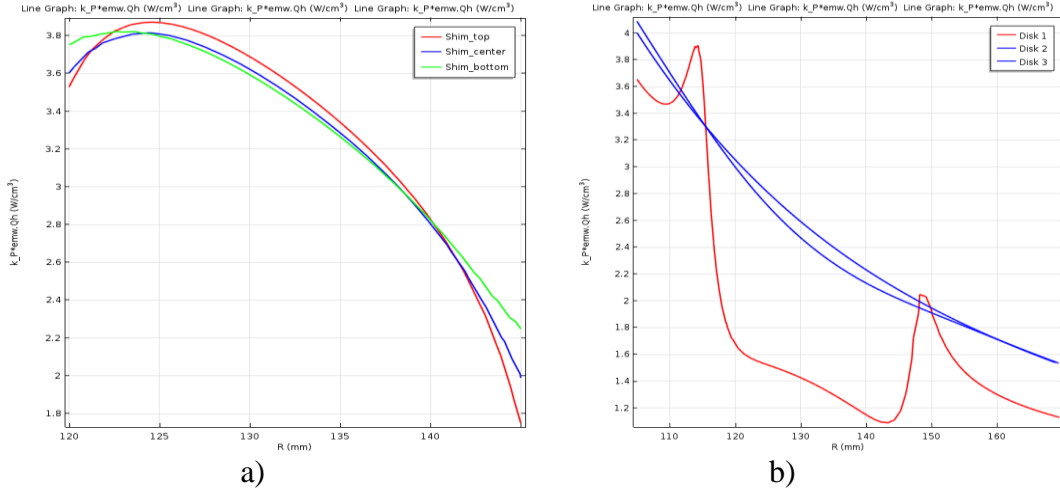


Fig. 8: RF loss power density in the shim (a) and in the disks (b) at the 17 kA bias

The distribution in Fig.8a can be expressed using the following formula

$$p = 3.85 - 0.059 \cdot (r[\text{mm}] - 125)^{1.9} \text{ W/cm}^3 \quad /5/$$

The distributions in Fig.8b can be expressed using the following formulae (mm and W/cm³)

Disk #1	$p = 1.4 \text{ W/cm}^3$	
Disk #1, addition	$p = 5.85 \text{ W/cm}^3$	/5/
Disks #2 and #3	$p = 7.68 - 0.037 \cdot r$	

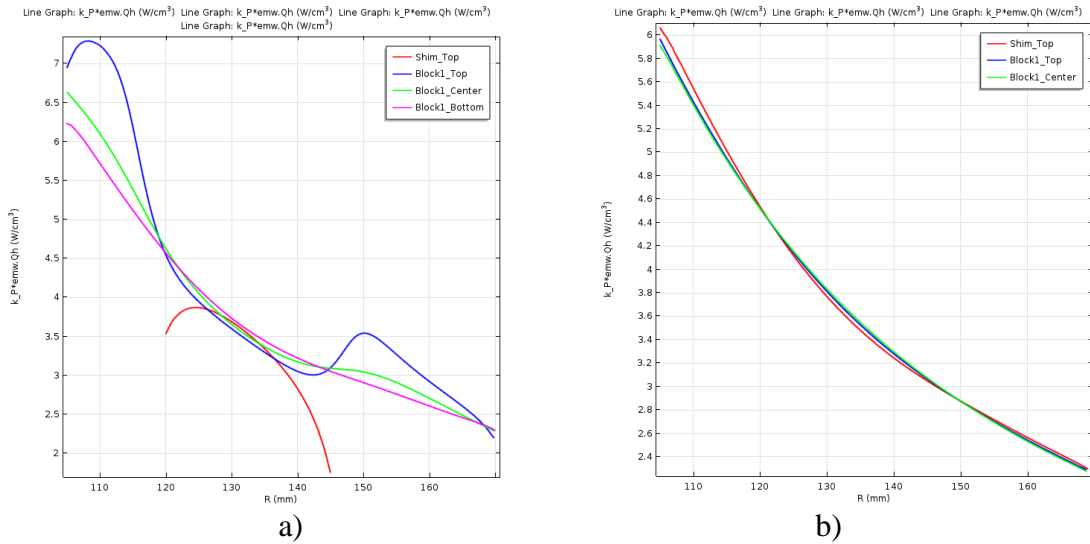


Fig. 9: RF loss power density in the block #1 (a) and in the block #2 (b) at 17 kA bias.

The distribution in Fig. 9a can be expressed using the following expression (mm and W/cm³)

$$p = 2.2 + 10^{-4} \cdot (180 - r)^{2.5} \quad /6/$$

The distribution in Fig. 9 b) can be expressed using the following expression (mm and W/cm³)

$$p = 6.35 - 0.055 \cdot r \quad /7/$$

As a result we can expand the data in Table 5 for the first 3-ms time range by adding the average energy deposition during the second 3-ms interval. Table 6 shows corresponding values in J/cm³. The last column of the table show the energy density deposited in the elements of the tuner during one accelerating cycle. As earlier, the radius is expressed in millimeters in this table.

Table 6. Energy density deposition in the elements of the tuner during one accelerating cycle.

Element	0 – 3 ms	16 – 19 ms	One acceleration cycle
Disk1	$10^{-3}*(23.3-0.111*r)$	4.2e-3	$10^{-3}*(27.5-0.111*r)$
Disk1_add	19.7e-3	17.6e-3	$10^{-3}*37.3$
Disk 2	$10^{-3}*(19.7-0.089*r)$	$10^{-3}*(23 - 0.111*r)$	$10^{-3}*(42.7-0.2*r)$
Disk 3	$10^{-3}*(12.3-0.055*r)$	$10^{-3}*(23 - 0.111*r)$	$10^{-3}*(35.3-0.166*r)$
Shim	23.6e-3	$10^{-3}*(11.6 - 0.0177*(r[mm] - 125)^{1.9})$	$10^{-3}*(35.2 - 0.0177*(r[mm] - 125)^{1.9})$
Shim_add	43.2e-3	$10^{-3}*(11.6 - 0.0177*(r[mm] - 125)^{1.9})$	$10^{-3}*(54.8 - 0.0177*(r[mm] - 125)^{1.9})$
Block1	$10^{-3}*(90-0.46*r)$	$10^{-3}*(6.6 + 3*10^{-4}*(180 - r)^{2.5})$	$10^{-3}*(96.6 - 0.46*r + 3*10^{-4}*(180 - r)^{2.5})$
Block1_1add	51e-3	$10^{-3}*(6.6 + 3*10^{-4}*(180 - r)^{2.5})$	$10^{-3}*(57.6 + 3*10^{-4}*(180 - r)^{2.5})$
Block1_2add	33e-3	$10^{-3}*(6.6 + 3*10^{-4}*(180 - r)^{2.5})$	$10^{-3}*(39.6 + 3*10^{-4}*(180 - r)^{2.5})$
Block2	$10^{-3}*(76.2 - 0.37*r)$	$10^{-3}*(19 - 0.165*r)$	$10^{-3}*(95.2 - 0.535*r)$

With the 15 Hz repetition rate, this energy deposition density per one cycle translates in the power density summarized in Table 7. In this table the radial dimension is in **centimeters**.

Table 7. Average RF loss power density deposition in the elements of the tuner (**cm**, W/cm³)

Element	
Disk1	$0.4125 - 1.67*10^{-2}*r$
Disk1_add	0.56
Disk 2	$0.64 - 0.03*r$
Disk 3	$0.53 - 0.025*r$
Shim	$0.53 - 0.0214 * r - 12.5 ^{1.9}$
Shim_add	$0.82 - 0.0214 * r - 12.5 ^{1.9}$
Block1	$1.45 - 0.069*r + 0.00133*(18.0 - r)^{2.5}$
Block1_add1	$0.864 + 0.00133*(180 - r)^{2.5}$
Block1_add2	$0.594 + 0.00133*(180 - r)^{2.5}$
Block2	$1.43 - 0.08*r$

Fig. 10 visualizes the data in Table 7 by showing distribution of the time-averaged RF loss power density in the elements of the tuner.

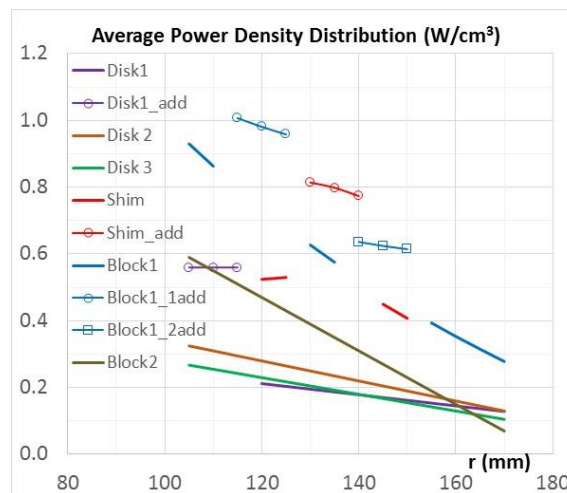


Fig. 10. Distribution of the average RF loss power density in the tuner

Before switching to solving the thermal problem, let's pay attention to the relatively high power deposition in the inner end of the Disk #1 (addition). As the alumina disk is not magnetic, high electrical field must be responsible for the power loss. This can mean a problem as the high electric field along the surface can lead to surface discharge effects. This problem will be further investigated later in this note.

The input for the thermal model shown in Fig. 11 was set using data in Table 7:

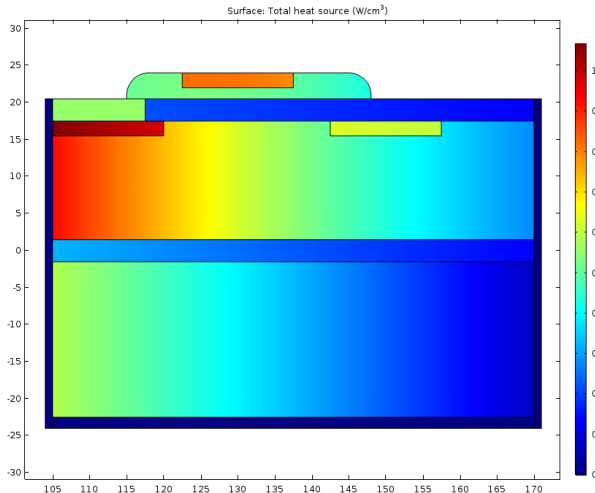


Fig. 11. A map of the power deposition in the upper part of the tuner (according to Table 7).

The temperature distribution in case when there is no thermal contact between the cylinder surfaces of the disks and cooling jacket is shown in Fig. 12a compared to the similar case, but without shim, in Fig 12b.

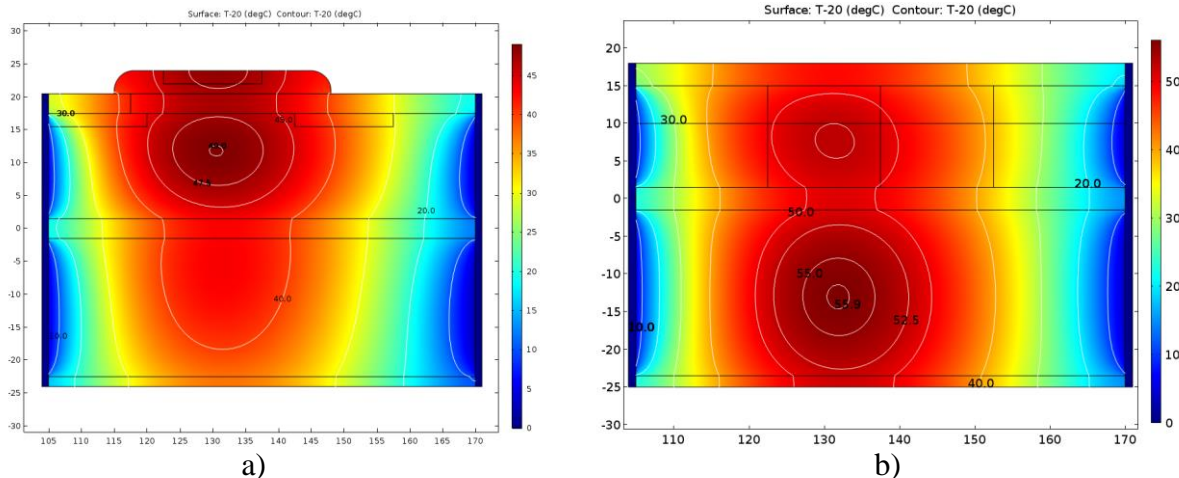


Fig. 12. Temperature map with no thermal contact on the inner and outer cylinder surfaces of the disks (a) compared with the results of the study in [4] with no shims (b).

The maximum temperature rise (49°C in the top block) now is ~7 degrees lower than it was in the previous design. If the case when the quality of thermal contact for the disks is the same as for the blocks, the temperature rise is 44°C (Fig. 13).

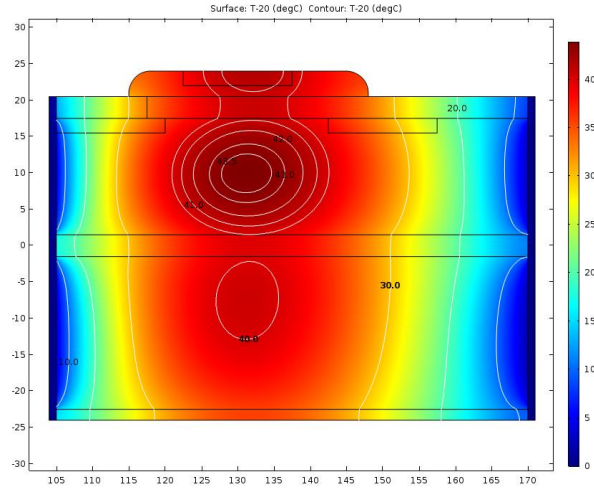


Fig. 13. Temperature map with uniform thermal contact on the inner and outer cylinder surfaces of the disks.

Electric field in the first alumina disk

As was mentioned earlier, anomalous heating of the first alumina disk is due to the elevated electric field between the shim and the inner electrode of the cavity. Fig. 14 shows static RF loss power density in the disk (a) and the values of the electric field in the area (b).

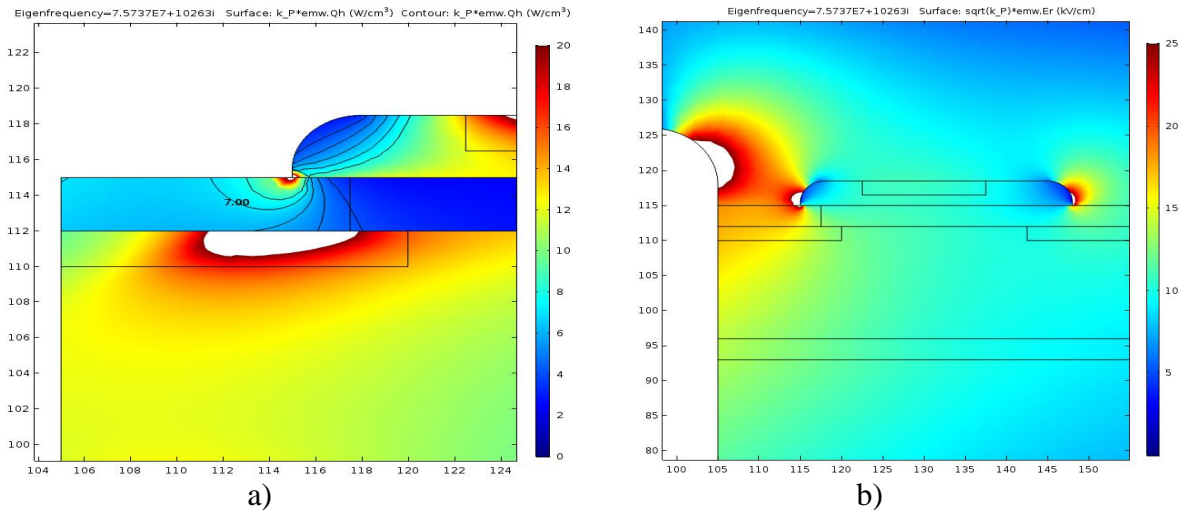


Fig. 14. Power deposition and the electric field in the 1-st disk

The maximum value of the radial component of the electric field on the surface of the disk in the triple point is ~40 kV/cm. It was possible to reduce this electric field by re-shaping the inner corner of the shim ring. The Figures 15 and 16 compare the magnetic field and the permeability at the lowest bias current $I_w = 6.6625$ kA for the initial shape of the shim and for the improved shape.

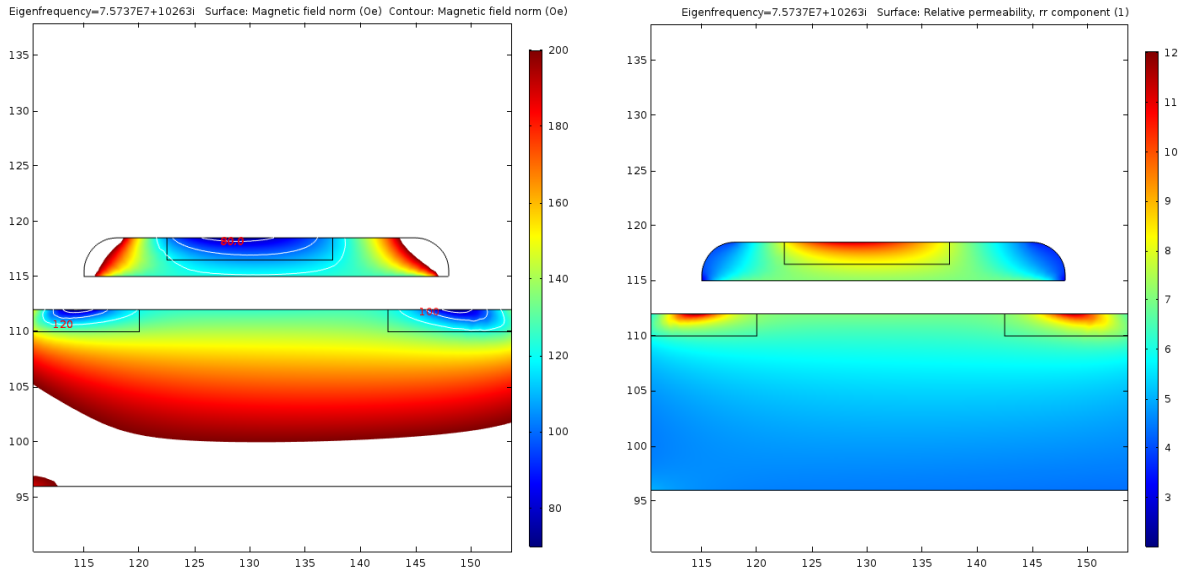


Fig. 15. Initial shape of the shim: minimum magnetic field is 67.3 Oe; maximum permeability is 12; maximum electric field along the surface is 40 kV/cm in the triple point.

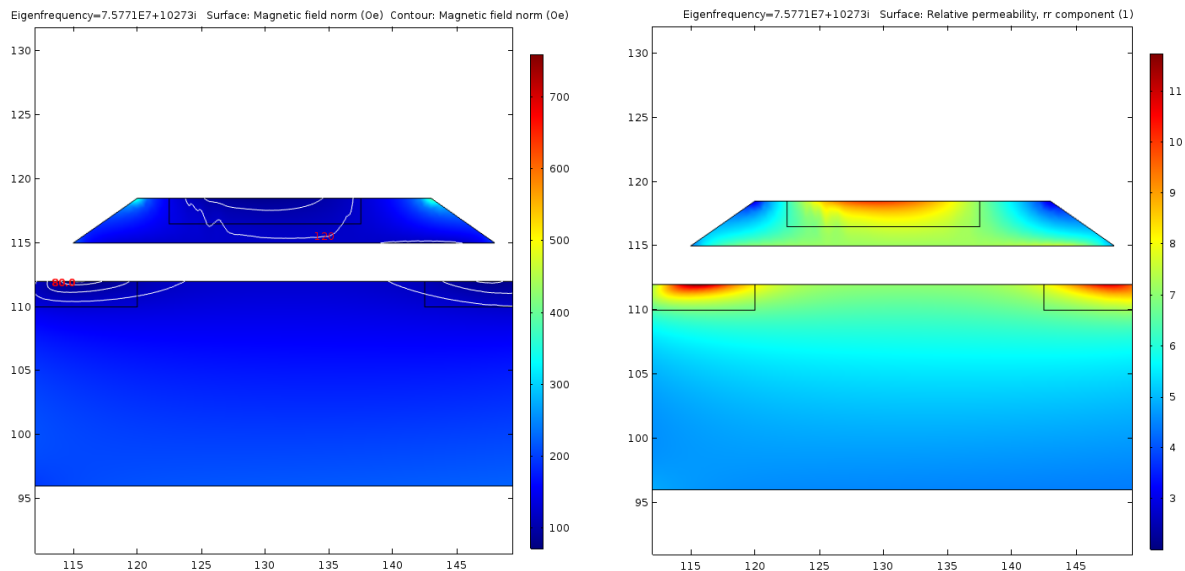


Fig. 16. Modified shape of the shim: minimum magnetic field is 69.3 Oe; maximum permeability is 11.75; maximum electric field along the surface is 27.5 kV/cm in the triple point.

After the geometry of the shim was modified to reduce the efficient permittivity, the minimum field became a bit higher – 69.3 Oe and the maximum permeability lower – 11.75. Electric field along the surface is now significantly smaller: 27.5 kV/cm. By making the inclination angle even smaller it was possible to further increase the minimum magnetic field up to ~71 Oe; in this case the maximum permeability became 11.5. Maximum radial electric field is now 25 kV/cm.

Summary.

By using internal magnetic shim, it was possible to significantly increase the minimum value of the magnetic field in the garnet material of the tuner. As a result, the maximum value of the RF loss power density became significantly smaller.

Possible increase of the surface electric field between the shim and the inner electrode of the cavity can be kept under control by appropriate shaping of the shim.

References

1. R. Madrak, et al, "Loss Tangent of AL-800 Garnet Material", FNAL TD note TD-15-005, April 2015.
2. R. Madrak, et al, "Permeability of AL-800 Garnet Material", FNAL TD note TD-15-014, June 2015.
3. I. Terechkine and G. Romanov, "Thermal Analysis of the Tuner of the FNAL Booster's 2-nd Harmonic Cavity", FNAL TD note TD-15-020, Oct. 2015.
4. I. Terechkine and G. Romanov, "Evaluation of Temperature Distribution in the Tuner of the FNAL Booster's Tunable Second Harmonic Cavity", FNAL TD note TD-16-002, February 2016.